HHS Public Access

Author manuscript

Annu Rev Chem Biomol Eng. Author manuscript; available in PMC 2019 June 07.

Published in final edited form as:

Annu Rev Chem Biomol Eng. 2018 June 07; 9: 229–252. doi:10.1146/annurev-chembioeng-060817-084034.

Biomolecular Ultrasound and Sonogenetics

David Maresca[1,*], **Anupama Lakshmanan**[2,*], **Mohamad Abedi**[2], **Avinoam Bar-Zion**[1], **Arash Farhadi**[2], **George J. Lu**[1], **Jerzy O. Szablowski**[1], **Di Wu**[3], **Sangjin Yoo**[1], and **Mikhail G. Shapiro**[1]

[1]Division of Chemistry and Chemical Engineering, California Institute of Technology, Pasadena, California 91125, USA

[2]Division of Biology and Biological Engineering, California Institute of Technology, Pasadena, California 91125, USA

[3]Division of Engineering and Applied Sciences, California Institute of Technology, Pasadena, California 91125, USA

Abstract

Visualizing and modulating molecular and cellular processes occurring deep within living organisms is fundamental to our study of basic biology and disease. Currently, the most sophisticated tools available to dynamically monitor and control cellular events rely on light-responsive proteins, which are difficult to use outside of optically transparent model systems, cultured cells, or surgically accessed regions owing to strong scattering of light by biological tissue. In contrast, ultrasound is a widely used medical imaging and therapeutic modality that enables the observation and perturbation of internal anatomy and physiology but has historically had limited ability to monitor and control specific cellular processes. Recent advances are beginning to address this limitation through the development of biomolecular tools that allow ultrasound to connect directly to cellular functions such as gene expression. Driven by the discovery and engineering of new contrast agents, reporter genes, and bioswitches, the nascent field of biomolecular ultrasound carries a wave of exciting opportunities.

Keywords

biomolecular; ultrasound; sonogenetics; gas vesicles; imaging; reporter gene

1. INTRODUCTION

Studying biological function within the context of living organisms and the development of biomolecular and cellular therapy requires methods to image and control the function of specific molecules and cells in vivo. However, most popular methods for achieving spatiotemporally precise interactions with biological substances, such as fluorescent imaging

*These authors contributed equally

DISCLOSURE STATEMENT

The authors are not aware of any affiliations, memberships, funding, or financial holdings that might be perceived as affecting the objectivity of this review.

and optogenetics, have limited utility in deep tissues owing to the strong scattering of visible light. Unlike photons, which are scattered within approximately one millimeter of tissue, ultrasound waves easily penetrate several centimeters deep while retaining spatial and temporal coherence. This capability has made ultrasound one of the world's leading modalities for medical imaging of anatomy, physiology, and noninvasive therapy. However, historically ultrasound has played a relatively small role in molecular and cell biology owing to a lack of effective methods to couple sound waves to specific processes such as gene expression and cellular signaling.

Recent advances are changing this picture by enabling ultrasound to image and control the function of specific biomolecules and cells and drive biomolecular transport across cellular and tissue barriers. These emerging capabilities for biomolecular ultrasound are the focus of this review. We start with a brief primer on ultrasound physics and technology. We then describe the development of genetically encodable acoustic biomolecules, which could serve as the ultrasound equivalents of fluorescent proteins for noninvasive molecular and cellular imaging. Next, we discuss proteins and genetic circuits allowing focused ultrasound (FUS) to remotely control gene expression and other aspects of cellular signaling through sonogenetic strategies analogous to optogenetics and chemogenetics. Finally, we discuss the role of ultrasound in enhancing the transport of biomolecules across cell membranes and tissue boundaries. We aim to convey both the exhilarating recent developments underlying the emergence of biomolecular ultrasound and the exciting opportunities this nascent field holds for creative biomolecular and ultrasound engineers.

2. BRIEF BACKGROUND ON BIOMEDICAL ULTRASOUND

2.1. Wave Behavior and Tissue Interactions

Ultrasound is defined by sound wave frequencies above those audible to humans (>20,000 Hz). Generated by transducers coupled to a transmission medium such as biological tissue, ultrasound waves travel through the medium and interact with its components to form images or provide momentum and energy for perturbation. In biological tissues, as in liquids, compression waves are dominant and are used for most modes of imaging and control. In tissue, sound waves travel at ~1,540 m/s and are reflected and scattered wherever they experience a change in acoustic impedance, which is a function of the local density and compressibility (1) (Figure 1*a*). The relative homogeneity of the speed of sound in soft tissues results in sound waves remaining coherent as they traverse the tissue, enabling simple image reconstruction without major aberrations (2). By comparison, visible light is strongly scattered in tissues, making it challenging for it to retain a ballistic path at depths greater than a few hundred microns (Figure 1*b*).

Ultrasound reflection at tissue interfaces is highly directional and reveals anatomical contours. Soft tissues have similar acoustic impedance values, resulting in relatively low contrast between them; air and bones have much lower and higher acoustic impedances, respectively, resulting in strong reflections (2). When the ultrasound wave encounters a target smaller than approximately one-tenth of the wavelength, it is scattered omnidirectionally (3). Biological tissues include a wide range of such scatterers in the form of fibers, cells, and organelles. The echo from a single scatterer is usually very weak. When

several very close scatterers are imaged, the result is a dominant spatially coherent interference pattern called speckle (2). The amplitude of the ultrasound wave decreases exponentially as a function of depth. Part of the energy of the ultrasonic wave is absorbed in the tissue and dissipated as heat. Attenuation refers to both absorption and any reduction in wave amplitude owing to reflection or scattering. Each tissue is characterized by a different attenuation coefficient value, which increases nonlinearly with frequency (2). As they pass through a medium, ultrasound waves also deposit momentum into that medium, resulting in mechanical forces known as acoustic radiation forces (ARF). Appreciable at higher ultrasound intensities and pulse durations, these forces, as well as localized heating, can be used to perturb and manipulate tissues and other materials.

2.2. Ultrasound Imaging

Ultrasound imaging is the most prescribed diagnostic modality in clinical practice (4). Typical equipment involves an ultrasound scanner and an ultrasound probe made of a linear array of transducer elements (i.e., 128 to 256 ultrasound transmitting/receiving elements) (5). Numerous ultrasound imaging modes have been translated to clinical practice; several of these modes are relevant to biomolecular ultrasound.

2.2.1. B-mode imaging—Ultrasound scanners are primarily used to produce real-time 2D images of underlying tissue (Figure 1*d*). These grayscale images are referred to as B-mode images (where B stands for brightness) and are acquired through transmission into a tissue of short ultrasound pulses and recording of backscattered echoes. The location of a scattering or reflecting source is reconstructed from the arrival time of its signal at each array element in a process known as beamforming. The position of a point in the reconstructed B-mode image depends on the time of flight of the echo and the position of the transmitting probe element. The in-depth or axial resolution of B-mode images depends on the wavelength ($\lambda = c_{tissue}/f_{US}$, where c is the speed of sound in tissue and f is the ultrasound wave frequency) and the number of cycles of vibration of the transmitted pulse. The axial resolution typically ranges from 500 μm (medical imaging) down to 50 μm (ultrasound biomicroscopy) (6). Because both attenuation and resolution increase with frequency, there is an inherent tradeoff between resolution and imaging depth (Figure 1*c*). The lateral resolution of B-mode images depends on the transmitted ultrasound beam width and is typically a few hundred microns. The transverse resolution or image thickness is usually on the order of a millimeter. B-mode imaging is used to image every organ of the body with the exception of bones or air-filled organs such as the lungs.

2.2.2. Doppler imaging—Ultrasound Doppler imaging detects the motion of red blood cells (RBCs) and, therefore, blood flow (7). RBCs scatter weak ultrasound echoes, which can be captured with modern ultrasound probes. At a given depth in tissue, the temporal shifts observed in consecutive RBC echoes allow detection of the displacement of RBCs and derivation of a Doppler signal proportional to RBC velocity. One can generate vascular images displaying either the velocity (color Doppler) or the energy of RBC echoes (power Doppler) (8).

2.2.3. Contrast imaging—Contrast-enhanced ultrasound relies on the administration of contrast agents to label specific aspects of anatomy or physiology. The conventional contrast agents used for this purpose are microbubbles: synthetic, micron-sized bubbles of gas stabilized by a lipid or protein shell (9–12). When injected into the blood stream, microbubbles produce strong scattering as they resonate at ultrasound imaging frequencies (1–20 MHz). Dedicated ultrasound contrast modes have been developed to benefit from that resonant behavior, such as amplitude modulation (13) or phase inversion (14), allowing the detection of microbubbles in vivo with higher specificity. Microbubbles can also be used to enhance Doppler imaging.

2.2.4. Ultrafast imaging—Conventional B-mode imaging uses a series of focused transmissions along an ultrasound array to form an image, such that the acquisition of a 10-cm-deep image with a 128-element probe takes at least 128 * 10 cm * 2/1,540 m/s ~ 17 ms, resulting in a frame rate of 59 Hz. A major recent advance, known as ultrafast ultrasound, uses single–plane wave transmissions, rather than focused line transmissions, to form images, resulting in a two-orders-of-magnitude acceleration in frame rate (15). The equivalent temporal resolution for a 10-cm image is 10 cm * 2/1,540 m/s ~ 130 μs, or 7,700 frames per second. This advance was made possible by improvements in computer hardware allowing flexible software beamforming. This technology was initially developed for shear wave elastography and later applied to Doppler imaging.

2.2.5. Functional ultrasound imaging—Ultrafast Doppler imaging has raised the sensitivity of conventional Doppler imaging by a factor of 30, leading to high-resolution, high–signal-to-noise ratio maps of the brain vasculature in rodents (16). The sequential acquisition of vascular maps of the brain with ultrafast Doppler has enabled the detection of neural activity through neurovascular coupling (17). Research efforts are ongoing to turn functional ultrasound imaging of the brain into a full-fledged neuroscience modality that complements functional magnetic resonance imaging (MRI) with improved spatiotemporal resolution, portability, and cost.

2.2.6. Ultrasound localization microscopy—Superresolution ultrasound imaging, also based on ultrafast ultrasound, was recently introduced using microbubbles as blinking sources. It was used to generate sub–10 μm–resolution images of the brain or tumors at the organ scale (Figure 1*d*) (18, 19).

To obtain 3D information, linear array transducers are typically translated in the transverse direction, acquiring multiple 2D planes. In the future, all the imaging modes described above could be translated into 3D with the use of dedicated ultrasound probes made of 2D arrays of transducers.

2.3. Focused Ultrasound Actuation

Thanks to the low attenuation of soft tissues, energy can be deposited at a specific location deep within the body using FUS (Figure 1*e*). Ultrasound can be applied based on known anatomical targeting or used under real-time guidance from magnetic resonance imaging (20), allowing accurate localization of the target site and monitoring effects on the tissue.

Ultrasound can be focused using either a curved single-element transducer or electronically focused multielement phased arrays, which in addition to steering the beam can correct for wave-front aberrations caused by acoustically mismatched tissues, such as the human skull (21).

There are three basic modes of ultrasound energy delivery (Figure 2): heat generation, exertion of ARF, and acoustic cavitation (22). Heating occurs owing to viscous dissipation as molecules move back and forth at the ultrasound focus, increasing with greater acoustic frequency and intensity. Reaching substantial temperature elevations typically requires pulse durations on the order of seconds. ARF in traveling ultrasound waves arises from the loss of momentum as sound waves become attenuated or reflected; by conservation, this momentum is transferred to particles in the medium. This effect scales with attenuation and usually requires pulses on the order of milliseconds for target tissues to reach their maximal elastic response to ARF. In addition to traveling waves, ARF can also arise in standing ultrasound waves owing to the presence of pressure nodes and antinodes, attracting or repelling particles based on their material properties (23). Finally, cavitation arises through the interaction of ultrasound with bubbles, which may arise spontaneously in the medium or become nucleated at material interfaces or are introduced as external cavitation agents (24). Cavitation can be stable, with gas bubbles periodically oscillating around their initial radius at the frequency of the acoustic wave, or inertial, in which rapid growth of the bubble followed by violent collapse releases large forces and fluid jets into surrounding media. Stable cavitation occurs preferentially at the resonance frequency of each bubble, with inertial cavitation becoming more likely with increases in the ratio between the peak negative pressure and the square root of the frequency—a ratio termed the mechanical index, with units of MPa MHz $^{-½}$ (1).

Each of these modes has been exploited for therapeutic purposes, such as thermal tissue ablation (25–28), local drug delivery (29–31), and thrombolysis (32), and has the potential to interact with biomolecules. Not covered in this review, unfocused ultrasound in the 20–100-kHz range is also widely used in laboratory and industrial processes to disrupt material structures, accelerate chemical processes, and clean surfaces. Most of these effects are thought to be mediated by cavitation (33).

2.4. Comparison of Ultrasound with Other Modalities for Imaging and Control

In comparison with other modalities for imaging and control of biological function, ultrasound provides exceptionally high temporal resolution with scalable, frequency-dependent spatial resolution and penetration depth. In addition, it offers a relatively wide variety of physical interactions for potential biomolecular coupling. Many of these unique advantages stem from fortuitous physical parameters. The density and compressibility of tissue lead to ultrasound wavelengths in the mid-micron range, whereas the relative homogeneity of tissue on this size scale leads to low scattering, enabling sound waves to penetrate deeply and be treated as coherent on their way in and out of the body. These characteristics also make it intrinsically straightforward to do things with ultrasound that may be harder with other modalities, such as pulse and wave-front shaping and superresolved signal reconstruction. In addition, the ability of ultrasound to deposit focused

momentum and energy in media allows it to interact with appropriate molecules, cells, and tissues through thermal and mechanical mechanisms.

However, ultrasound does have some limitations compared with other methods. For instance, its ability to penetrate bony enclosures and air-filled compartments is limited compared with magnetic resonance and radioactive techniques. Furthermore, although the spatial precision of ultrasound can be scaled with frequency, achieving a (nonsuper-)spatial resolution approaching optical imaging (~1 μm) would require using a frequency (1.5 GHz) (34) that is readily attenuated within less than 1 mm of tissue, obviating a key advantage of ultrasound compared with optical methods. Most importantly for the purpose of this review, ultrasound currently has far fewer biomolecular tools to connect it to cellular and molecular function. However, as addressed in the following sections, new tools are starting to emerge to address this gap.

3. BIOMOLECULAR CONTRAST AGENTS AND REPORTER GENES FOR ULTRASOUND

3.1. Gas Vesicles

For several decades, micron-sized synthetic bubbles have been used as ultrasound contrast agents, leading to important preclinical and clinical applications (9–11). Although these bubbles can be functionalized to recognize and bind to specific targets in the bloodstream, their size and limited in vivo stability make it challenging to use them for molecular imaging of extravascular targets and monitoring of dynamic cellular processes. In 2014, a unique class of gas-filled proteins called gas vesicles were introduced as the first biomolecular contrast agents for ultrasound, paving the way for more direct visualization of cellular and molecular function using sound waves (35).

3.1.1. Basic biology and history of gas vesicles as ultrasound reporters—Gas vesicles (GVs) were initially identified in 1965 as components of gas vacuoles found in cyanobacteria (36), themselves first observed in 1895 as intracellular bodies whose native function is to regulate cellular buoyancy for optimal access to light and nutrients (37). GVs of different shapes and sizes have been identified in a variety of bacteria and archaea and have been studied by pioneering biology groups to determine their basic genetic, structural, physical, and biochemical properties (38, 39). GVs are cylindrical or spindle-shaped protein nanostructures, with lengths ranging from 100 nm to 2 μm and widths of 45–200 nm (Figure 3*a,b*). GVs comprise a 2-nm-thick amphiphilic shell that allows gas from the surrounding media to freely permeate in and out of their hollow interior, while excluding the aqueous phase. This amphiphilicity is accomplished by the primary structural constituent of GVs, a ~7.5-kDa protein called GvpA, which is predicted to fold into a beta sheet structure with hydrophobic and hydrophilic faces (40) (Figure 3*c*). In addition to GvpA, a cluster of 7–13 other genes is needed to enable GV production (Figure 3*d*), encoding minor structural proteins and assembly factors such as chaperones and nucleators (38, 39).

GVs are a remarkable product of evolution. First, whereas nanoscale bubbles are highly unstable owing to their high Laplace pressure, GVs are fundamentally physically stable and

in equilibrium with their surroundings; gas dissolved in surrounding media equilibrates with the contents of GVs on a microsecond timescale (41). Second, despite having a ratio of ~75:1 between their diameter and shell thickness, GVs can withstand pressures of up to 1.3 MPa before collapsing (38). Third, the entire GV structure, with a molecular weight in the range of ~50–350 MDa, is self-assembled mostly from a single 7.5-kDa protein repeated in its shell in a highly ordered arrangement.

The first demonstration of GVs as acoustic biomolecules, published in 2014, showed that GVs from *Anabaena flos-aquae* (Ana) and *Halobacterium salinarum NRC-1* (Halo) could produce ultrasound contrast in their purified form, inside cells, and after injection in vivo (Figure 3*e*), opening the door to their development as biomolecular reporters for ultrasound and as targeted nanoscale agents for molecular imaging (35). The GVs were detectable at concentrations below 12 pM (corresponding to ~3.5 μg/ml or 0.005% volume fraction) (35, 42). This initial study provided a glimpse of the potential of GVs to serve as background-subtracted imaging agents based on their ability to collapse at specific acoustic pressures, the ability to distinguish multiple GV types for multiplexing, and their production of nonlinear acoustic signals. Since then, considerable progress has been made in understanding and engineering the acoustic properties of GVs, enhancing the ability of ultrasound to detect them, and developing them as acoustic reporter genes (42–46).

3.1.2. Understanding and engineering the acoustic and targeting properties of gas vesicles—From the perspective of biomolecular engineering, the genetic encodability of GVs raises the possibility of tuning the properties of these acoustic contrast agents at the level of their DNA sequence and constituent proteins. The outer shell of GVs is composed almost entirely of GV proteins A and C (GvpA and GvpC). GvpA is a ~7.5-kDa amphiphilic protein that composes the primary GV shell material, whereas GvpC forms the outer scaffold that influences shape and structural integrity (Figure 3*d*) (38, 39).

In 2016, a versatile molecular engineering platform based on GvpC was established to modify the mechanical, acoustic, surface, and targeting properties of purified Ana GVs (43). This platform was based on removing the wild-type GvpC bound to Ana GV shells and replacing it with genetically engineered versions of this protein. This is done conveniently by treating Ana GVs with 6-M urea to remove its native GvpC and incubating the stripped GVs with new GvpC proteins expressed recombinantly in *Escherichia coli* (Figure 3*f*). Unbound molecules are removed by repeated separation of GVs via centrifugally assisted flotation. This modular approach allows the testing and use of many different GvpC variants on the same stripped GV backbone (Figure 3*g*).

Based on GvpC's large influence on GV shell mechanics (38), engineering this protein enables modulation of the way GVs respond to and scatter ultrasound (43). For example, it allows tuning of the pressure at which GVs collapse and thereby lose their ultrasound contrast, enabling multiplexed imaging through serial collapse (Figure 3*h*). The direct relationship established between hydrostatic and acoustic GV collapse pressures provides a convenient method to evaluate GV modifications to generate tuned variants (43). In addition to mechanical tuning, GvpC can be used as a genetic handle for GV functionalization to achieve cell-specific molecular targeting, tuning of GV uptake by macrophages, and

multimodal imaging with ultrasound and fluorescence (Figure 3*g*). GvpC functionalization is achieved by direct fusion of the relevant peptides, or via a bio-orthogonal covalent attachment using the SpyTag-SpyCatcher protein assembly system. Genetic fusion to GvpC has also been used to develop GVs as antigen display particles (47).

Although initial engineering efforts have primarily focused on substituting one component of GVs purified from native hosts with genetically engineered versions, an alternative strategy would be to engineer GVs entirely at the level of their DNA sequence and express these modified gene clusters in native or heterologous hosts. Natural GVs come in a variety of shapes, sizes, and collapse pressures depending on their microbial origin (38, 39). A rational genetic engineering approach combining elements from different native GV gene clusters, or making functionally conservative mutations in certain GV genes, could be used to engineer hybrid or mutant GVs that display unique mechanical and acoustic phenotypes. Such mutations have been shown in basic studies to produce a variety of GV shape phenotypes (48–50). This aspect is further explored in the context of developing acoustic reporter genes, as elaborated in a later section.

3.1.3. Gas vesicle mechanics and pulse sequences for imaging them—Among the most useful properties of GVs for ultrasound imaging is their nonlinear mechanical response to ultrasound. This response was originally observed as backscattering at harmonics of the excitation frequency and was understood in subsequent studies as the product of nonlinear buckling deformations of the GV shell (44, 45) (Figure 3*i*). In these studies, finite element modeling of two types of single GVs predicted the existence of a pressure-dependent buckling behavior of the GV shell at the applied acoustic frequency, with these step changes in GV volume resulting in harmonic scattering (Figure 3*j*). This buckling takes place only above a threshold pressure specific to each GV type, which can be tuned through genetic engineering (45). Remarkably, these buckling deformations are fully reversible when they take place at megahertz frequencies, allowing GVs to respond to thousands of ultrasound cycles every second. This reversibility is aided by the inability of GV-contained gas to exit the shell on a sub-microsecond timescale, so that it becomes compressed after buckling and resists the total collapse of GVs (44). Pressures that produce buckling under ultrasound tend to collapse GVs irreversibly when applied hydrostatically, as this quasistatic compression allows gas molecules to exit the GV during pressurization, with the shell carrying the full compressive load by itself.

The specific nondestructive detection of GVs in vivo against anatomical background is key to ensuring the success of GVs as ultrasound reporters. Toward this end, an imaging approach was recently developed to take advantage of GVs' nonlinear buckling behavior. This technique uses an amplitude modulation (AM) sequence that detects differential backscattering generated by two consecutive transmissions of different amplitudes, with the stronger and weaker pulses above and below the buckling threshold, respectively (45). AM produced greater GV contrast specificity and was used to distinguish engineered GVs from linear scatterers in vitro (Figure 3*k*) and in vivo.

Mechanical modeling of GVs also yielded an estimate of the scattering cross section of single GVs (44). For Halo GVs, this cross section was similar to that of a RBC at 20 MHz,

despite the GV being 4,500 times smaller (volumes of 20 aL for a GV and 90 pL for a RBC).

3.1.4. Development of acoustic reporter genes—The discovery of GVs as acoustic biomolecules raises the potential of their development as acoustic reporter genes (ARGs), which could do for ultrasound what green fluorescent protein (GFP) and its derivatives have done for optical imaging. Development of ARGs requires functional heterologous expression of GV operons, which was initially pursued in commensal and therapeutic microbes as a means to image their location and function inside mammalian hosts—an important capability for basic microbiome research and biomedical synthetic biology. In the first study to introduce ARGs, *E. coli* and *Salmonella typhimurium* cells were genetically engineered to produce ultrasound image contrast (46) (Figure 4*a*). This development required engineering a hybrid GV gene cluster with components from two organisms. This was necessitated by the observations that the transfer of GV gene clusters from organisms producing known echogenic GVs (Ana and Halo) did not result in GV production in *E. coli.* At the same time, the expression of a known *E. coli*–compatible GV gene cluster from *Bacillus megaterium* (51) produced small GVs conferring little to no ultrasound contrast to their host cells. The solution was to combine the structural proteins GvpA and GvpC from Ana with the assembly factors from *B. megaterium*. This resulted in cells with strong ultrasound contrast corresponding to their expression of this hybrid operon, which was named ARG1 (Figure 4*a*).

On average, cells transformed to express ARG1 produced 100 GVs per cell, accounting for approximately 10% of their intracellular volume (Figure 4*b*). Placed downstream from a chemically inducible promoter, these cells produced ultrasound contrast corresponding to the expected transfer function of the inducer (Figure 4*c,d*). By using appropriate promoters, ARGs were adapted to a range of microbes, such as probiotic bacterial strain *E. coli* Nissle 1917 (EcN) and the medically relevant attenuated *S. typhimurium* strain ELH1301. The spatial distribution of EcN-expressing ARGs could be imaged with ultrasound in the mouse colon (Figure 4*e*); their spatial arrangement was more clearly delineated compared with the diffuse optical signals generated by EcN cells expressing a bioluminescent reporter.

An important aspect of reporter genes is the ability to multiplex different colors of the reporter (e.g., blue and green fluorescent protein) to visualize multiple cell types or molecular signals. Following the strategy used with purified GVs, genetic modification of GvpC in the ARG1 cluster resulted in intracellular GVs with different acoustic collapse pressures, allowing duplex imaging (46). Future genetic engineering of ARGs will also benefit from high-throughput screening to develop variants with new acoustic or biochemical properties. Toward this end, bacterial colonies containing ARG plasmids can be imaged with ultrasound directly on agar plates, allowing rapid detection of different ARG phenotypes.

Beyond the development of ARGs for microbial imaging, there is a strong impetus to develop ARGs for mammalian cells, as this would allow the imaging of mammalian gene expression and tracking of the location and function of cellular therapeutics. Toward this end, a major effort is under way to transfer the genetic machinery encoding GVs from

prokaryotes to eukaryotes. This effort represents a significant synthetic biology challenge owing to the large number of genes involved in the operon, the importance of their stoichiometry, and the requirement that the proteins they encode find each other and self-assemble inside the cell.

3.2. Alternative Biomolecular Reporters for Ultrasound

In addition to GVs, other possibilities could be explored as potential sources of biomolecular and genetically encodable ultrasound contrast. One possible reporter gene mechanism involves local accumulation of synthetic microbubble contrast agents in tissues expressing a biorthogonal binding group. Turnbull and colleagues (52) pioneered this approach by transfecting cells with an engineered transmembrane protein displaying an extracellular peptide substrate for biotinylation, together with an endoplasmic reticulum–targeted biotin ligase enzyme. This resulted in the display of biotin on the surface of cells. Transgenic mice expressing this construct under the control of a vascular promoter displayed biotin on their vascular endothelium, leading to accumulation of intravenous avidin-functionalized microbubbles, which were visualized with ultrasound.

Another possibility involves local generation of bubbles with gas-producing enzymes. Mattrey and collaborators (53, 54) showed that 200–500-nm silica nanoparticles loaded with catalase, which produces water and molecular oxygen from H_2O_2, can generate ultrasound-visible bubbles in peroxide-rich media and tissues. Although free bubbles generated via this mechanism are physically unstable, they had apparent lifetimes of several minutes in tissue, allowing imaging. This constitutes an example of an active molecular sensor (of peroxide) for ultrasound and raises the possibility that a gas-producing enzyme such as catalase could serve as a reporter gene. However, this possibility entails questions about the availability of reactants, the kinetics of gas formation and dissolution, and the potential impact of the enzymatic activity and free bubble formation on the cell. Finally, although they are outside the scope of this review, emerging synthetic technologies, such as perfluorocarbon nanodroplets that become converted to microscale bubbles after exposure to ultrasound (55), could be used as synthetic labels for cells or as extravasating targeted contrast agents.

4. SONOGENETIC ACTUATION OF CELLULAR SIGNALING

FUS has a long history of use as a therapeutic modality, with current applications primarily focused on localized ablation of deep tissue targets (25–28). However, ultrasound's ability to be focused and deliver energy to a site of interest with millimeter precision could also be used to provide an input signal for biomolecular and cellular signaling. For example, ultrasound's ability to controllably elevate temperature by several degrees Celsius under image guidance could provide a safe, rapid, reversible signal for biomolecular actuation. In addition, its ability to apply mechanical forces to tissues and scattering objects could be harnessed to control mechanical signaling. Coupled to appropriate genetically encoded molecular constructs, this would provide sonogenetic control of cellular function, analogous to optogenetic and chemogenetic techniques, which use optical and chemical inputs. Specific examples would be the excitability of specific neurons, the proliferation of microbes in the gut, or the release of cell-expressing therapeutic payloads.

4.1. Thermally Mediated Ultrasonic Control

A wide array of thermal bioswitches have the potential to translate elevations in temperature into biochemical reactions that control cellular signaling and/or the expression of specific genes. These switches include heat shock promoters (56), temperature-sensitive ion channels (57), riboswitches (58), and heat-responsive transcription repressors (59, 60).

Pioneering studies on temperature-mediated responses to ultrasound have focused on the mammalian heat shock promoter HSP70, whose induction upon FUS has been linked to several genetic outputs, including the expression of reporter genes (61), suicide genes (62), and cytokines (63). HSP70 is a good starting point for thermal control because it is tightly repressed in the off state and rapidly inducible after only a few minutes of stimulation at 43°C, with the potential to reach several thousand-fold induction (64, 65). However, HSP70 can also respond to other stress stimuli, such as hypoxia, glucose starvation, and viral infection (66), which renders controlling gene expression solely via changes in temperature more challenging. Moreover, thermal induction of HSPs is transient and varies among cell types; therefore, it is ineffective in some cell types, such as neurons (67, 68). Finally, in bacteria, heat shock promoters have a fairly modest dynamic range and also respond pleiotropically (69, 70).

Recently, a new class of tunable, orthogonal temperature-dependent transcriptional repressors was engineered to enable the next generation of sonogenetic thermal bioswitches (71) (Figure 5*a*). These switches use engineered versions of the orthogonal bacterial transcriptional repressors TlpA and TcI, which have sharp transition temperatures (3–4°C) and more than 300-fold induction. These switches were engineered using directed evolution to have tunable set-points within the biomedically relevant temperature range of 32–46°C. They have been integrated into thermal logic circuits to perform complex functions, such as multiplexing and bandpass activation, and provide precise control over the spatiotemporal profile and dose of gene expression. Spatially precise activation of these circuits with FUS was demonstrated in bacterial culture phantoms and inside mammalian hosts with a brief thermal pulse (71). Unlike other bioswitches, these proteins respond solely to temperature elevations, with a sharp transition that can be tuned for specific applications. Combining these molecular devices with synthetic biology circuits may advance the use of FUS beyond simple transient switches to more complex functions, such as sustained, multiplexed, and on-off switching.

Nontranscriptional responses to ultrasound based on temperature may also be possible. For example, magnetic and optical hyperthermia have been used in conjunction with temperature-sensitive ion channels (72–76). Unfortunately, most temperature-sensitive channels also respond to other inputs and depend on cellular states such as membrane potential and pH. RNA thermometers could provide thermal responses at the translational level, but these switches typically suffer from a broad thermal transition, with relatively small fold changes and leaky expression at baseline (58).

4.2. Mechanical Actuation of Receptors

As a complement to thermal approaches, ARFs applied to cells could be used to actuate mechanical signaling. For example, ultrasound amplified by microbubbles can be used to control mechanosensitive signaling elements, such as ion channels. This concept was first demonstrated in vitro, where ultrasound triggered the opening of the *E. coli*–derived mechanosensitive ion channel MscL heterologously expressed in mammalian cells (77) (Figure 5*b*). Subsequently, the endogenous mechanosensitive channel Trp4 was stimulated in the worm *Caenorhabditis elegans*, in a study that also introduced the term sonogenetics (78). More recently, the Piezo1 mechanosensitive ion channel was expressed in HEK293T and immune cells and perturbed using a microbubble-mediated acoustic mechanism for remote-controlled gene activation (79). Whereas the kinetics typically associated with thermal actuation are on the order of seconds, mechanical actuation can operate on millisecond timescales, potentially enabling control of cell signaling with higher temporal precision. However, techniques that require microbubbles are limited in their mammalian applications owing to the difficulty of delivering bubbles out of the blood stream. Several recent studies have reported effects on mechanosensitive ion channels in vitro in the absence of microbubbles (80, 81); however, the potential involvement of fluid streaming in these phenomena may make them less likely to be applicable in vivo.

4.3. Ultrasonic Neuromodulation

Another emerging use of ultrasound in biophysical systems is the excitation or inhibition of neural activity. Compared with established neuromodulation techniques, such as transcranial magnetic stimulation, transcranial electrical stimulation, deep brain stimulation, infrared stimulation, and optogenetics, ultrasonic neuromodulation (UNM) offers unique advantages as a noninvasive technique that can be focused deeply and precisely inside the brain. The concept and modern use of UNM were advanced by Fry and colleagues (82) in the 1950s and Tyler and colleagues (83, 84) in 2008, respectively, followed by studies in multiple labs demonstrating the effects of ultrasound on movement behavior and neural signaling. UNM is typically performed with relatively low frequencies (0.25~0.7 MHz) to facilitate transmission through the skull and low intensities (<100 W cm^{-2} averaged over the pulse train) to minimize the possibility of side effects, such as cavitation and heating (85, 86). Parameters leading to motor and sensory responses have been examined in species ranging from mice (87–90) to humans (91, 92).

A major issue facing the UNM field is lack of knowledge about the biomolecular, cellular, and neural circuit mechanisms underpinning this technique. For example, there is contradictory evidence about whether the motor responses elicited by UNM are the result of direct modulation of the motor cortex or a by-product of sensory activation. Recently, two independent groups have demonstrated that UNM can produce off-target sensory responses in mice (93) and guinea pigs (94) owing to indirect effects on the auditory system. Although the frequencies used in UNM are inaudible, they may produce mechanical vibrations or shear waves in the brain and skull that can be transmitted to the ears. Deafening of the animals confirmed that this effect is likely responsible for some of the motor behaviors attributed in the literature to direct UNM stimulation. These findings are consistent with

historical reports of somatosensory and auditory percepts owing to ultrasound in humans (95, 96).

At the same time, several studies with in vitro preparations have reported the ability of UNM to directly stimulate or inhibit neurons. In an early study, Tyler et al. (83) found that ultrasound is capable of opening voltage-gated ion channels to evoke action potentials in brain slices, and it was hypothesized that the mechanical effect of ultrasound might change the viscoelastic properties of the cell membrane and kinetics of membrane-bound proteins (80, 97, 98). In a theoretical study, Shoham and colleagues (99) suggested that UNM is mediated by the nucleation and cavitation of bubbles inside the lipid bilayer. However, this mechanism has not been confirmed experimentally, and detailed biophysical studies are needed to fully elucidate how ultrasound affects neuronal excitability. Once a mechanistic understanding is obtained, the UNM strategy could be optimally tuned for direct, spatially selective control of human brain function, and neurons could be genetically modified to strengthen their response to ultrasound for sonogenetic applications.

5. ULTRASOUND-ASSISTED BIOMOLECULAR TRANSPORT

A final mechanism by which ultrasound can interact with biomolecules is by enhancing their transport through cellular and tissue barriers. This mechanism typically relies on the cavitational behavior of microbubbles to translate applied ultrasound fields into local strain on a scale much smaller than the ultrasound wavelength.

5.1. Cellular Sonoporation

Sonoporation is the process of creating pores in cell membranes using ultrasound to facilitate the transport of molecules into or out of the cell (Figure 6*a*). Both stable and inertial cavitation have been used for this purpose. Stably vibrating bubbles can potentially create pores by pushing or pulling on the membranes of adjacent cells (100). In addition, stable cavitation creates acoustic microstreaming that can assist in propelling drugs into cells (100). Meanwhile, inertial cavitation results in the implosion of the microbubble and the formation of jets, leading to membrane disruption (101). By focusing the ultrasound beam at the desired location, these mechanisms can improve the delivery of molecules such as drugs (102) and genes (103) into target cells.

5.2. Vascular Barrier Opening

Delivering biomolecules and other substances to the central nervous system poses a particular challenge owing to the blood-brain barrier (BBB), an endothelial tissue with specialized tight junctions, which limits the physical transport of molecules from the blood into the brain. Additionally, vascular cells in the BBB are less permeable owing to their reduced number of fenestrations, less-efficient pinocytosis, and expression of efflux pumps. While the BBB protects the brain from unwanted metabolites and pathogens, its consequence for neuroscience and neuropsychiatric medicine is that only small, lipophilic molecules are typically capable of entering the brain from the bloodstream, limiting the tools available for research and therapy. Work over the past two decades has demonstrated that FUS applied transcranially after an intravenous administration of microbubbles results in

temporary blood-brain barrier opening (BBBO) at the ultrasound focus, allowing localized trans-BBB delivery of intravascularly injected molecules within the first 6–24 h after insonation (Figure 6*b*) (30, 104). This effect is mediated by stable cavitation exerting pressure on the endothelial wall (105, 106) and has been shown to enable targeted delivery of small molecules (30), proteins (107), and viruses (108).

The efficiency of molecule delivery depends on several factors, including the ultrasound pressure and size of the molecule. The ultrasound pressure necessary to open the BBB increases proportionally to the ultrasound frequency (109), with higher frequencies (above ~1.5 Mhz) and pressures carrying greater risk of skull heating. Most studies avoid crossing the inertial cavitation threshold of microbubbles to avoid tissue damage and hemorrhage that can occur during a microbubble collapse (110). FUS-BBBO has been shown to be safe when used below the inertial cavitation threshold (111), and it is currently undergoing clinical trials (29).

Larger biomolecules, such as adeno-associated viral vectors (~20-nm diameter), require higher ultrasound pressures than small molecules or proteins to achieve comparable delivery, often close to the inertial cavitation threshold (112). Currently, efficient delivery of adeno-associated viral vectors and nanoparticles requires a careful balance between efficacy and safety owing to the possibility of hemorrhage and tissue damage (112, 113). These issues can be alleviated by real-time monitoring of inertial cavitation, allowing fine-tuning of pressures for each brain site (114).

As a noninvasive technique capable of targeting viral vectors to a specific region of the brain, FUS-BBBO creates an unprecedented opportunity for noninvasive control of neural activity with spatial, temporal, and cell-type specificity. These aspects were recently combined in a technique called acoustically targeted chemogenetics (ATAC) (115), which uses FUS-BBBO to deliver viral vectors to specific brain regions, using cell-specific promoters to target selected populations of cells within those regions and encoding chemogenetic receptors—proteins that respond exclusively to bioinert drugs (116)—to gain temporal control of the targeted cells. ATAC holds significant advantages over typical neuropsychiatric drugs, which act indiscriminately throughout the brain with limited regional and cellular specificity. With viral gene delivery in humans undergoing clinical trials (117), ATAC has potential for future clinical translation.

5.3. Acoustic Trapping and Manipulation of Cells and Molecules

In addition to direct biomolecular actuation, ARF can be used to trap and manipulate objects with appropriate size and acoustic contrast relative to surrounding media. This effect has been used extensively in vitro to separate and trap micron-scale particles and mammalian cells for cell sorting and visualization (118, 119). Often, these approaches rely on standing acoustic waves in microfluidic devices to create pressure nodes and antinodes serving as stable attractors for the particles (Figure 6*c*). The potential for in vivo translation of ARF has also been demonstrated by the manipulation of RBCs inside a blood vessel (120, 121). One limitation of ARF is its inability to manipulate objects smaller than approximately a few microns, owing to a more dominant force that arises from acoustic streaming (122, 123).

Careful engineering of the streaming pattern can itself be used to trap nanoparticles in vitro (124, 125), but this may be difficult to realize in a complex environment, such as in vivo.

6. MULTIMODAL IMAGING USING BIOMOLECULES

In addition to its direct use as a single modality, ultrasound can be combined with other forms of energy, such as light and magnetic fields, to enable the imaging or actuation of biomolecules. These approaches are briefly described below.

6.1. Photoacoustic Imaging

Photoacoustic imaging (PAI) is based on the physical coupling of light and sound. In PAI, short laser pulses produce local thermoelastic expansion in a light-absorbing region of tissue, which serves as a source of acoustic waves, which are detected by an ultrasound transducer coupled to the skin (126, 127). PAI combines optical contrast and spectral specificity with improved penetration depth. However, this penetration depth is still smaller than that of ultrasound imaging (127).

Endogenous PAI uses light absorption by biomolecules such as hemoglobin (128) and melanin (129), which are intrinsically present in the organism. Multiwavelength imaging and spectral unmixing allow PAI to differentiate between several materials at the same location. For example, it can measure oxygen saturation based on the difference between the absorption spectra of deoxygenated and oxygenated hemoglobin (130). In addition to endogenous sources, molecular contrast agents have been engineered to enable molecular PAI in vivo (131–134).

6.2. Acoustically Modulated Light Focusing

Another useful coupling between ultrasound and light is in the emerging area of scattering correction. Because light scattering is a coherent process, photons can be focused through an opaque tissue using optical phase conjugation (135, 136) or focused into static tissue using iterative wave front shaping (137). However, this focusing requires an internal guide star to determine the needed phase distribution. In acoustically modulated light-focusing methods, this guide star is produced by modulating the light propagating through an acoustic focus using the acousto-optic effect (138). Light selectively modulated at the ultrasound focus is time reversed and transmitted back into the desired focus location (139). By using acoustically modulated light focusing, focused fluorescent imaging can be performed at a depth of 2.5 mm inside scattering tissue (140). Finally, the system resolution can be increased beyond the size of the ultrasound focal point, achieving lateral resolution of ~5 μm (141). Despite the promise of these methods, one significant limitation to their applications in living tissues is the rapid decoherence of scatterers owing to tissue motion relative to the timescales involved in focusing.

6.3. Acoustically Modulated Magnetic Resonance

The capabilities of biomolecular ultrasound could be expanded through coupling to an orthogonal noninvasive imaging modality such as MRI, which has advantages in terms of its penetration through bone-enclosed structures, such as the skull. For example, an MRI

contrast agent that can be modulated with sound waves would stand out against other background sources of contrast, enabling more specific and sensitive imaging. This kind of coupling was recently demonstrated using GVs, which, in addition to their ability to scatter and be collapsed by ultrasound, have been shown to produce two types of MRI contrast. These include hyperpolarized xenon MRI based on their gas-exchange properties (142) and proton susceptibility–based MRI enabled by the differential magnetic susceptibility of the GV-contained gas and the surrounding aqueous media, which creates a nanoscale magnetic field gradient around each GV particle (143). The latter study also demonstrated that acoustically collapsing GVs in situ erases the GV-specific MRI contrast. Subtracting the images taken before and after insonation, the endogenous tissue contrast can be removed. Additional benefits of GV-based acoustically modulated MRI include multiplexed imaging combining GVs with different acoustic collapse pressures, reporter gene imaging using ARG constructs, and clustering-based molecular functional imaging.

7. OUTLOOK

In summary, ultrasound is a versatile modality for observing and perturbing biological function in living organisms, with intrinsic advantages owing to its fundamental physics and tissue interactions. The field of biomolecular ultrasound and sonogenetics seeks to connect these physics to the function of specific biomolecules and cells to enable precise imaging and control of cellular processes. This is being accomplished by identifying and engineering biomolecular agents with the appropriate properties to interact with sound waves or their resultant thermal and mechanical effects. Although this field is in its infancy, the recent development of bacterial GVs as the first acoustic biomolecules and reporter genes for ultrasound promises to connect this imaging modality to in vivo cell biology, analogously to the function performed for optical imaging by fluorescent proteins. At the same time, new developments in temperature-sensitive and mechanosensitive biomolecules, as well as improved understanding of the biophysical basis of UNM, open the door to precise sonogenetic control analogous to optogenetics and chemogenetics. In parallel, the use of ultrasound to enhance or pattern the transport of proteins, genes, and viruses across cellular and vascular boundaries creates new opportunities to deploy advanced biomolecular tools in biological and clinical scenarios.

Much work remains to be done before these nascent technologies will have a major impact in biology or medicine. For example, the gene clusters encoding GVs must be transferred to a larger variety of organisms, including mammalian cells, for them to serve as versatile acoustic reporter genes. To facilitate sensitive detection of these proteins in vivo, their acoustic properties must be optimized in tandem with ultrasound techniques to maximally distinguish their signals from background. In parallel, a high priority for sonogenetics is to eliminate the need for synthetic microbubbles as actuators of mechanosensitive signaling. To date, only thermal approaches can truly be considered sonogenetic—using fully genetically encoded components. In the future, microbubbles could be replaced with genetically encoded actuators, and insights from the study of UNM could identify direct mechanisms for cellular coupling to ultrasound not requiring any such actuator. Finally, to enable the use of ultrasound to influence a broader range of transport phenomena in vivo, it would be

useful to develop methods to nucleate bubbles for cavitation in situ. As biomolecular engineers, we face these challenges with buoyant excitement.

Acknowledgments

The authors thank members of the Shapiro laboratory and collaborators for helpful discussions. Related work in the Shapiro laboratory is supported by the Heritage Medical Research Institute, the National Institutes of Health, the Defense Advanced Research Projects Agency, the Jacobs Institute for Molecular Engineering in Medicine, the Caltech Center for Environmental Microbial Interactions, the Human Frontiers Science Program, the Burroughs Wellcome Fund, the Pew Scholarship in the Biomedical Sciences, the Sontag Foundation, and the Packard Fellowship for Science and Engineering. D.M. is supported by a postdoctoral fellowship from the Human Frontier Science Program. A.L. and M.A. are supported by the National Science Foundation graduate research fellowship.

LITERATURE CITED

1. Szabo TL. Diagnostic Ultrasound Imaging: Inside Out. Cambridge, MA: Academic; 2004.
2. Azhari H. Basics of Biomedical Ultrasound for Engineers. Hoboken, NJ: John Wiley & Sons; 2010.
3. Cobbold RS. Foundations of Biomedical Ultrasound. Oxford, UK: Oxford Univ. Press; 2006.
4. Liang H-D, Noble JA, Wells PNT. Recent advances in biomedical ultrasonic imaging techniques. Interface Focus. 2011; 1:475–76.
5. Powers J, Kremkau F. Medical ultrasound systems. Interface Focus. 2011; 1:477–89. [PubMed: 22866226]
6. Foster FS, Pavlin CJ, Harasiewicz KA, Christopher DA, Turnbull DH. Advances in ultrasound biomicroscopy. Ultrasound Med Biol. 2000; 26:1–27. [PubMed: 10687788]
7. Evans DH, Jensen JA, Nielsen MB. Ultrasonic colour Doppler imaging. Interface Focus. 2011; 1:490–502. [PubMed: 22866227]
8. Rubin JM, Bude RO, Carson PL, Bree RL, Adler RS. Power Doppler US: a potentially useful alternative to mean frequency-based color Doppler US. Radiology. 1994; 190:853–56. [PubMed: 8115639]
9. Ferrara K, Pollard R, Borden M. Ultrasound microbubble contrast agents: fundamentals and application to gene and drug delivery. Annu Rev Biomed Eng. 2007; 9:415–47. [PubMed: 17651012]
10. Paefgen V, Doleschel D, Kiessling F. Evolution of contrast agents for ultrasound imaging and ultrasound-mediated drug delivery. Front Pharmacol. 2015; 6:197. [PubMed: 26441654]
11. Unnikrishnan S, Klibanov AL. Microbubbles as ultrasound contrast agents for molecular imaging: preparation and application. Am J Roentgenol. 2012; 199:292–99. [PubMed: 22826389]
12. Frinking PJA, Bouakaz A, Kirkhorn J, Ten Cate FJ, de Jong N. Ultrasound contrast imaging: current and new potential methods. Ultrasound Med Biol. 2000; 26:965–75. [PubMed: 10996696]
13. Mor-Avi V, Caiani EG, Collins KA, Korcarz CE, Bednarz JE, Lang RM. Combined assessment of myocardial perfusion and regional left ventricular function by analysis of contrast-enhanced power modulation images. Circulation. 2001; 104:352–57. [PubMed: 11457757]
14. Simpson DH, Chin CT, Burns PN. Pulse inversion Doppler: a new method for detecting nonlinear echoes from microbubble contrast agents. IEEE Trans Ultrason Ferroelectr Freq Control. 1999; 46:372–82. [PubMed: 18238434]
15. Tanter M, Fink M. Ultrafast imaging in biomedical ultrasound. IEEE Trans Ultrason Ferroelectr Freq Control. 2014; 61:102–19. [PubMed: 24402899]
16. Mace E, Montaldo G, Osmanski BF, Cohen I, Fink M, Tanter M. Functional ultrasound imaging of the brain: theory and basic principles. IEEE Trans Ultrason Ferroelectr Freq Control. 2013; 60:492–506. [PubMed: 23475916]
17. Mace E, Montaldo G, Cohen I, Baulac M, Fink M, Tanter M. Functional ultrasound imaging of the brain. Nat Methods. 2011; 8:662–64. [PubMed: 21725300]
18. Errico C, Pierre J, Pezet S, Desailly Y, Lenkei Z, et al. Ultrafast ultrasound localization microscopy for deep super-resolution vascular imaging. Nature. 2015; 527:499–502. [PubMed: 26607546]

19. Lin F, Shelton SE, Espíndola D, Rojas JD, Pinton G, Dayton PA. 3-D ultrasound localization microscopy for identifying microvascular morphology features of tumor angiogenesis at a resolution beyond the diffraction limit of conventional ultrasound. Theranostics. 2017; 7:196–204. [PubMed: 28042327]
20. Hynynen K, Darkazanli A, Unger E, Schenck JF. MRI-guided noninvasive ultrasound surgery. Med Phys. 1993; 20:107–15. [PubMed: 8455489]
21. Hynynen K, Clement GT, McDannold N, Vykhodtseva N, King R, et al. 500-Element ultrasound phased array system for noninvasive focal surgery of the brain: a preliminary rabbit study with ex vivo human skulls. Magn Reson Med. 2004; 52:100–7. [PubMed: 15236372]
22. O'Brien WD. Ultrasound-biophysics mechanisms. Prog Biophys Mol Biol. 2007; 93:212–55. [PubMed: 16934858]
23. Sarvazyan AP, Rudenko OV, Nyborg WL. Biomedical applications of radiation force of ultrasound: historical roots and physical basis. Ultrasound Med Biol. 2010; 36:1379–94. [PubMed: 20800165]
24. Coussios CC, Roy RA. Applications of acoustics and cavitation to noninvasive therapy and drug delivery. Annu Rev Fluid Mech. 2008; 40:395–420.
25. Jolesz FA, Hynynen K, McDannold N, Tempany C. MR imaging-controlled focused ultrasound ablation: a noninvasive image-guided surgery. Magn Reson Imaging Clin N Am. 2005; 13:545–60. [PubMed: 16084419]
26. Hesley GK, Gorny KR, Woodrum DA. MR-guided focused ultrasound for the treatment of uterine fibroids. Cardiovasc Interv Radiol. 2013; 36:5–13.
27. Uchida T, Nakano M, Hongo S, Shoji S, Nagata Y, et al. High-intensity focused ultrasound therapy for prostate cancer. Int J Urol. 2012; 19:187–201. [PubMed: 22188161]
28. Illing RO, Kennedy JE, Wu F, ter Haar GR, Protheroe AS, et al. The safety and feasibility of extracorporeal high-intensity focused ultrasound (HIFU) for the treatment of liver and kidney tumours in a Western population. Br J Cancer. 2005; 93:890–95. [PubMed: 16189519]
29. Carpentier A, Canney M, Vignot A, Reina V, Beccaria K, et al. Clinical trial of blood-brain barrier disruption by pulsed ultrasound. Sci Transl Med. 2016; 8:343re2.
30. Hynynen K, McDannold N, Vykhodtseva N, Jolesz FA. Noninvasive MR imaging-guided focal opening of the blood-brain barrier in rabbits. Radiology. 2001; 220:640–46. [PubMed: 11526261]
31. Machet L, Boucaud A. Phonophoresis: efficiency, mechanisms and skin tolerance. Int J Pharm. 2002; 243:1–15. [PubMed: 12176291]
32. Bader KB, Bouchoux G, Holland CK. Sonothrombolysis. Adv Exp Med Biol. 2016; 880:339–62. [PubMed: 26486347]
33. Mason T, Lorimer J. Applied Sonochemistry. Weinheim, Ger: Wiley-VCH Verlag; 2002.
34. Brand S, Weiss EC, Lemor RM, Kolios MC. High frequency ultrasound tissue characterization and acoustic microscopy of intracellular changes. Ultrasound Med Biol. 2008; 34:1396–407. [PubMed: 18439747]
35. Shapiro MG, Goodwill PW, Neogy A, Yin M, Foster FS, et al. Biogenic gas nanostructures as ultrasonic molecular reporters. Nat Nanotechnol. 2014; 9:311–16. [PubMed: 24633522]
36. Bowen C, Jensen T. Blue-green algae: fine structure of the gas vacuoles. Science. 1965; 147:1460–62. [PubMed: 17776627]
37. Klebahn H. Gasvakuolen, ein Bastendteil der Zellen der wasserblutenbildenden Phycochromaceen. Flora. 1895; 80:241–82.
38. Walsby A. Gas vesicles. Microbiol Rev. 1994; 58:94–144. [PubMed: 8177173]
39. Pfeifer F. Distribution, formation and regulation of gas vesicles. Nat Rev Microbiol. 2012; 10:705–15. [PubMed: 22941504]
40. Ezzeldin HM, Klauda JB, Solares SD. Modeling of the major gas vesicle protein, GvpA: from protein sequence to vesicle wall structure. J Struct Biol. 2012; 179:18–28. [PubMed: 22580065]
41. Walsby AA, Revsbech NP, Grieffel DH. The gas permeability coefficient of the cyanobacterial gas vesicle wall. J Gen Microbiol. 1992; 138:837–45.
42. Lakshmanan A, Lu GJ, Farhadi A, Nety SP, Kunth M, et al. Preparation of biogenic gas vesicle nanostructures for use as contrast agents for ultrasound and MRI. Nat Protoc. 2017; 12:2050. [PubMed: 28880278]

43. Lakshmanan A, Farhadi A, Nety SP, Lee-Gosselin A, Bourdeau RW, et al. Molecular engineering of acoustic protein nanostructures. ACS Nano. 2016; 10:7314–22. [PubMed: 27351374]
44. Cherin E, Melis JM, Bourdeau RW, Yin M, Kochmann DM, et al. Acoustic behavior of *Halobacterium salinarum* gas vesicles in the high-frequency range: experiments and modeling. Ultrasound Med Biol. 43:1016–30.
45. Maresca D, Lakshmanan A, Lee-Gosselin A, Melis JM, Ni Y-L, et al. Nonlinear ultrasound imaging of nanoscale acoustic biomolecules. Appl Phys Lett. 2017; 110:073704. [PubMed: 28289314]
46. Bourdeau RW, Lee-Gosselin A, Lakshmanan A, Farhadi A, Kumar SR, et al. Acoustic reporter genes for non-invasive imaging of microbes in mammalian hosts. Nature. 2018; 553:86–90. [PubMed: 29300010]
47. Stuart ES, Morshed F, Sremac M, DasSarma S. Cassette-based presentation of SIV epitopes with recombinant gas vesicles from halophilic archaea. J Biotechnol. 2004; 114:225–37. [PubMed: 15522433]
48. Offner S, Wanner G, Pfeifer F. Functional studies of the gvpACNO operon of *Halobacterium salinarium* reveal that the GvpC protein shapes gas vesicles. J Bacteriol. 1996; 178:2071–78. [PubMed: 8606186]
49. Offner S, Ziese U, Wanner G, Typke D, Pfeifer F. Structural characteristics of halobacterial gas vesicles. Microbiology. 1998; 144:1331–42. [PubMed: 9611808]
50. Strunk T, Hamacher K, Hoffgaard F, Engelhardt H, Zillig MD, et al. Structural model of the gas vesicle protein GvpA and analysis of GvpA mutants *in vivo*. Mol Microbiol. 2011; 81:56–68. [PubMed: 21542854]
51. Li N, Cannon MC. Gas vesicle genes identified in *Bacillus megaterium* and functional expression in *Escherichia coli*. J Bacteriol. 1998; 180:2450–58. [PubMed: 9573198]
52. Bartelle BB, Berrios-Otero CA, Rodriguez JJ, Friedland AE, Aristizábal O, Turnbull DH. Novel genetic approach for in vivo vascular imaging in mice. Circ Res. 2012; 110:938–47. [PubMed: 22374133]
53. Olson ES, Orozco J, Wu Z, Malone CD, Yi B, et al. Toward *in vivo* detection of hydrogen peroxide with ultrasound molecular imaging. Biomaterials. 2013; 34:8918–24. [PubMed: 23958028]
54. Malone CD, Yeh Y, Esener S, Mattrey R, Hoyt K. Proc Ultrason Symp, Tours, Fr. New York: IEEE Int; 2016. Ultrasound characterization of oxygen contrast agents produced during the reaction of hydrogen peroxide with catalase-loaded nanoparticles; 1–4.
55. Sheeran PS, Luois SH, Mullin LB, Matsunaga TO, Dayton PA. Design of ultrasonically-activatable nanoparticles using low boiling point perfluorocarbons. Biomaterials. 2012; 33:3262–69. [PubMed: 22289265]
56. Leung TK, Rajendran MY, Monfries C, Hall C, Lim L. The human heat-shock protein family. Expression of a novel heat-inducible HSP70 (HSP70B') and isolation of its cDNA and genomic DNA. Biochem J. 1990; 267:125–32. [PubMed: 2327978]
57. Dhaka A, Viswanath V, Patapoutian A. TRP ion channels and temperature sensation. Annu Rev Neurosci. 2006; 29:135–61. [PubMed: 16776582]
58. Hoynes-O'Connor A, Hinman K, Kirchner L, Moon TS. *De novo* design of heat-repressible RNA thermosensors in *E. coli*. Nucleic Acids Res. 2015; 43:6166–79. [PubMed: 25979263]
59. Valdez-Cruz NA, Caspeta L, Pérez NO, Ramírez OT, Trujillo-Roldán MA. Production of recombinant proteins in *E. coli* by the heat inducible expression system based on the phage lambda pL and/or pR promoters. Microb Cell Fact. 2010; 9:18. [PubMed: 20298615]
60. Hurme R, Berndt KD, Normark SJ, Rhen M. A proteinaceous gene regulatory thermometer in *Salmonella*. Cell. 1997; 90:55–64. [PubMed: 9230302]
61. Madio DP, van Gelderen P, DesPres D, Olson AW, de Zwart JA, et al. On the feasibility of MRI-guided focused ultrasound for local induction of gene expression. J Magnet Reson Imaging. 1998; 8:101–4.
62. Braiden V, Ohtsuru A, Kawashita Y, Miki F, Sawada T, et al. Eradication of breast cancer xenografts by hyperthermic suicide gene therapy under the control of the heat shock protein promoter. Hum Gene Ther. 2000; 11:2453–63. [PubMed: 11119417]

63. Xiong X, Sun Y, Sattiraju A, Jung Y, Mintz A, et al. Remote spatiotemporally controlled and biologically selective permeabilization of blood-brain barrier. J Control Release. 2015; 217:113–20. [PubMed: 26334482]
64. Deckers R, Quesson B, Arsaut J, Eimer S, Couillaud F, Moonen CT. Image-guided, noninvasive, spatiotemporal control of gene expression. PNAS. 2009; 106:1175–80. [PubMed: 19164593]
65. Guilhon E, Voisin P, de Zwart JA, Quesson B, Salomir R, et al. Spatial and temporal control of transgene expression *in vivo* using a heat-sensitive promoter and MRI-guided focused ultrasound. J Gene Med. 2003; 5:333–42. [PubMed: 12692867]
66. Anckar J, Sistonen L. Regulation of HSF1 function in the heat stress response: implications in aging and disease. Annu Rev Biochem. 2011; 80:1089–115. [PubMed: 21417720]
67. Batulan Z, Shinder GA, Minotti S, He BP, Doroudchi MM, et al. High threshold for induction of the stress response in motor neurons is associated with failure to activate HSF1. J Neurosci. 2003; 23:5789–98. [PubMed: 12843283]
68. Oehler R, Pusch E, Zellner M, Dungel P, Hergovics N, et al. Cell type-specific variations in the induction of hsp70 in human leukocytes by feverlike whole body hyperthermia. Cell Stress Chaperones. 2001; 6:306–15. [PubMed: 11795467]
69. de Marco A, Vigh L, Diamant S, Goloubinoff P. Native folding of aggregation-prone recombinant proteins in *Escherichia coli* by osmolytes, plasmid- or benzyl alcohol–overexpressed molecular chaperones. Cell Stress Chaperones. 2005; 10:329–39. [PubMed: 16333986]
70. Zhao K, Liu M, Burgess RR. The global transcriptional response of *Escherichia coli* to induced σ^{32} protein involves σ^{32} regulon activation followed by inactivation and degradation of σ^{32} *in vivo*. J Biol Chem. 2005; 280:17758–68. [PubMed: 15757896]
71. Piraner DI, Abedi MH, Moser BA, Lee-Gosselin A, Shapiro MG. Tunable thermal bioswitches for *in vivo* control of microbial therapeutics. Nat Chem Biol. 2017; 13:75–80. [PubMed: 27842069]
72. Stanley SA, Sauer J, Kane RS, Dordick JS, Friedman JM. Remote regulation of glucose homeostasis in mice using genetically encoded nanoparticles. Nat Med. 2015; 21:92–98. [PubMed: 25501906]
73. Huang H, Delikanli S, Zeng H, Ferkey DM, Pralle A. Remote control of ion channels and neurons through magnetic-field heating of nanoparticles. Nat Nano. 2010; 5:602–6.
74. Chen R, Romero G, Christiansen MG, Mohr A, Anikeeva P. Wireless magnetothermal deep brain stimulation. Science. 2015; 347:1477–80. [PubMed: 25765068]
75. Yoo S, Kim R, Park J-H, Nam Y. Electro-optical neural platform integrated with nanoplasmonic inhibition interface. ACS Nano. 2016; 10:4274–81. [PubMed: 26960013]
76. Carvalho-de-Souza JL, Treger JS, Dang B, Kent SBH, Pepperberg DR, Bezanilla F. Photosensitivity of neurons enabled by cell-targeted gold nanoparticles. Neuron. 2015; 86:207–17. [PubMed: 25772189]
77. Heureaux J, Chen D, Murray VL, Deng CX, Liu AP. Activation of a bacterial mechanosensitive channel in mammalian cells by cytoskeletal stress. Cell Mol Bioeng. 2014; 7:307–19. [PubMed: 25606062]
78. Ibsen S, Tong A, Schutt C, Esener S, Chalasani SH. Sonogenetics is a non-invasive approach to activating neurons in *Caenorhabditis elegans*. Nat Commun. 2015; 6:8264. [PubMed: 26372413]
79. Pan Y, Yoon S, Sun J, Huang Z, Lee C, et al. Mechanogenetics for the remote and noninvasive control of cancer immunotherapy. PNAS. 2018; 115:992–97. [PubMed: 29343642]
80. Kubanek J, Shi J, Marsh J, Chen D, Deng C, Cui J. Ultrasound modulates ion channel currents. Sci Rep. 2016; 6:24170. [PubMed: 27112990]
81. Prieto ML, Firouzi K, Khuri-Yakub BT, Maduke M. Activation of Piezo1 but not Nav1.2 channels by ultrasound at 43 MHz. bioRxiv preprint. 2017.
82. Fry FJ, Ades HW, Fry WJ. Production of reversible changes in the central nervous system by ultrasound. Science. 1958; 127:83–84. [PubMed: 13495483]
83. Tyler WJ, Tufail Y, Finsterwald M, Tauchmann ML, Olson EJ, Majestic C. Remote excitation of neuronal circuits using low-intensity, low-frequency ultrasound. PLOS ONE. 2008; 3:e3511. [PubMed: 18958151]
84. Tufail Y, Matyushov A, Baldwin N, Tauchmann ML, Georges J, et al. Transcranial pulsed ultrasound stimulates intact brain circuits. Neuron. 2010; 66:681–94. [PubMed: 20547127]

85. Naor O, Krupa S, Shoham S. Ultrasonic neuromodulation. J Neural Eng. 2016; 13:031003. [PubMed: 27153566]
86. Dalecki D. Mechanical bioeffects of ultrasound. Annu Rev Biomed Eng. 2004; 6:229–48. [PubMed: 15255769]
87. Mehic E, Xu JM, Caler CJ, Coulson NK, Moritz CT, Mourad PD. Increased anatomical specificity of neuromodulation via modulated focused ultrasound. PLOS ONE. 2014; 9:e86939. [PubMed: 24504255]
88. Yang PS, Kim H, Lee W, Bohlke M, Park S, et al. Transcranial focused ultrasound to the thalamus is associated with reduced extracellular GABA levels in rats. Neuropsychobiology. 2012; 65:153–60. [PubMed: 22378299]
89. Bystritsky A, Korb AS, Douglas PK, Cohen MS, Melega WP, et al. A review of low-intensity focused ultrasound pulsation. Brain Stimul. 2011; 4:125–36. [PubMed: 21777872]
90. Deffieux T, Younan Y, Wattiez N, Tanter M, Pouget P, Aubry JF. Low-intensity focused ultrasound modulates monkey visuomotor behavior. Curr Biol. 2013; 23:2430–33. [PubMed: 24239121]
91. Legon W, Sato TF, Opitz A, Mueller J, Barbour A, et al. Transcranial focused ultrasound modulates the activity of primary somatosensory cortex in humans. Nat Neurosci. 2014; 17:322–29. [PubMed: 24413698]
92. Lee W, Kim H, Jung Y, Song IU, Chung YA, Yoo SS. Image-guided transcranial focused ultrasound stimulates human primary somatosensory cortex. Sci Rep. 2015; 5:8743. [PubMed: 25735418]
93. Sato T, Shapiro MG, Tsao DY. Ultrasonic neuromodulation causes widespread cortical activation via an indirect auditory mechanism. bioRxiv preprint. 2018.
94. Guo H, Hamilton M, Offutt SJ, Gloeckner CD, Li T. , et al. Ultrasound produces extensive brain activation via a cochlear pathway. bioRxiv preprint. 2018.
95. Legon W, Rowlands A, Opitz A, Sato TF, Tyler WJ. Pulsed ultrasound differentially stimulates somatosensory circuits in humans as indicated by EEG and FMRI. PLOS ONE. 2012; 7:e51177. [PubMed: 23226567]
96. Pumphrey RJ. Upper limit of frequency for human hearing. Nature. 1950; 166:571.
97. Tyler WJ. Noninvasive neuromodulation with ultrasound? A continuum mechanics hypothesis. Neuroscientist. 2011; 17:25–36. [PubMed: 20103504]
98. Prieto ML, Omer O, Khuri-Yakub BT, Maduke MC. Dynamic response of model lipid membranes to ultrasonic radiation force. PLOS ONE. 2013; 8:e77115. [PubMed: 24194863]
99. Plaksin M, Shoham S, Kimmel E. Intramembrane cavitation as a predictive bio-piezoelectric mechanism for ultrasonic brain stimulation. Phys Rev X. 2014; 4:011004.
100. Marmottant P, Hilgenfeldt S. Controlled vesicle deformation and lysis by single oscillating bubbles. Nature. 2003; 423:153–56. [PubMed: 12736680]
101. Prentice P, Cuschieri A, Dholakia K, Prausnitz M, Campbell P. Membrane disruption by optically controlled microbubble cavitation. Nat Phys. 2005; 1:107–10.
102. Kotopoulis S, Dimcevski G, Gilja OH, Hoem D, Postema M. Treatment of human pancreatic cancer using combined ultrasound, microbubbles, and gemcitabine: a clinical case study. Med Phys. 2013; 40:072902. [PubMed: 23822453]
103. Sirsi SR, Borden MA. Advances in ultrasound mediated gene therapy using microbubble contrast agents. Theranostics. 2012; 2:1208–22. [PubMed: 23382777]
104. Choi JJ, Pernot M, Small SA, Konofagou EE. Noninvasive, transcranial and localized opening of the blood-brain barrier using focused ultrasound in mice. Ultrasound Med Biol. 2007; 33:95–104. [PubMed: 17189051]
105. Hosseinkhah N, Hynynen K. A three-dimensional model of an ultrasound contrast agent gas bubble and its mechanical effects on microvessels. Phys Med Biol. 2012; 57:785–808. [PubMed: 22252221]
106. Tung YS, Vlachos F, Feshitan JA, Borden MA, Konofagou EE. The mechanism of interaction between focused ultrasound and microbubbles in blood-brain barrier opening in mice. J Acoust Soc Am. 2011; 130:3059–67. [PubMed: 22087933]

107. Samiotaki G, Acosta C, Wang S, Konofagou EE. Enhanced delivery and bioactivity of the neurturin neurotrophic factor through focused ultrasound-mediated blood–brain barrier opening *in vivo*. J Cereb Blood Flow Metab. 2015; 35:611–22. [PubMed: 25586140]
108. Thevenot E, Jordao JF, O'Reilly MA, Markham K, Weng YQ, et al. Targeted delivery of self-complementary adeno-associated virus serotype 9 to the brain, using magnetic resonance imaging-guided focused ultrasound. Hum Gene Ther. 2012; 23:1144–55. [PubMed: 22838844]
109. McDannold N, Vykhodtseva N, Hynynen K. Blood-brain barrier disruption induced by focused ultrasound and circulating preformed microbubbles appears to be characterized by the mechanical index. Ultrasound Med Biol. 2008; 34:834–40. [PubMed: 18207311]
110. Poon C, McMahon D, Hynynen K. Noninvasive and targeted delivery of therapeutics to the brain using focused ultrasound. Neuropharmacology. 2017; 120:20–37. [PubMed: 26907805]
111. Downs ME, Buch A, Sierra C, Karakatsani ME, Teichert T, et al. Long-term safety of repeated blood-brain barrier opening via focused ultrasound with microbubbles in non-human primates performing a cognitive task. PLOS ONE. 2015; 10:e0125911. [PubMed: 25945493]
112. Chen H, Konofagou EE. The size of blood-brain barrier opening induced by focused ultrasound is dictated by the acoustic pressure. J Cereb Blood Flow Metab. 2014; 34:1197–204. [PubMed: 24780905]
113. Song KH, Fan AC, Hinkle JJ, Newman J, Borden MA, Harvey BK. Microbubble gas volume: a unifying dose parameter in blood-brain barrier opening by focused ultrasound. Theranostics. 2017; 7:144–52. [PubMed: 28042323]
114. O'Reilly MA, Hynynen K. Blood-brain barrier: real-time feedback-controlled focused ultrasound disruption by using an acoustic emissions-based controller. Radiology. 2012; 263:96–106. [PubMed: 22332065]
115. Szablowski JO, Lue B, Lee-Gosselin A, Malounda D, Shapiro MG. Acoustically targeted chemogenetics for noninvasive control of neural circuits. bioRxiv preprint. 2018.
116. Sternson SM, Roth BL. Chemogenetic tools to interrogate brain functions. Annu Rev Neurosci. 2014; 37:387–407. [PubMed: 25002280]
117. Keeler AM, ElMallah MK, Flotte TR. Gene therapy 2017: progress and future directions. Clin Transl Sci. 2017; 10:242–48. [PubMed: 28383804]
118. Laurell T, Petersson F, Nilsson A. Chip integrated strategies for acoustic separation and manipulation of cells and particles. Chem Soc Rev. 2007; 36:492–506. [PubMed: 17325788]
119. Evander M, Nilsson J. Acoustofluidics 20: applications in acoustic trapping. Lab Chip. 2012; 12:4667–76. [PubMed: 23047553]
120. Dyson M, Woodward B, Pond JB. Flow of red blood cells stopped by ultrasound. Nature. 1971; 232:572–73. [PubMed: 4937504]
121. Galanzha EI, Viegas MG, Malinsky TI, Melerzanov AV, Juratli MA, et al. *In vivo* acoustic and photoacoustic focusing of circulating cells. Sci Rep. 2016; 6:21531. [PubMed: 26979811]
122. Barkholt Muller P, Barnkob R, Herring Jensen MJ, Bruus H. A numerical study of microparticle acoustophoresis driven by acoustic radiation forces and streaming-induced drag forces. Lab Chip. 2012; 12:4617–27. [PubMed: 23010952]
123. Barnkob R, Augustsson P, Laurell T, Bruus H. Acoustic radiation- and streaming-induced microparticle velocities determined by microparticle image velocimetry in an ultrasound symmetry plane. Phys Rev E. 2012; 86:056307.
124. Antfolk M, Muller PB, Augustsson P, Bruus H, Laurell T. Focusing of sub-micrometer particles and bacteria enabled by two-dimensional acoustophoresis. Lab Chip. 2014; 14:2791–99. [PubMed: 24895052]
125. Mao Z, Li P, Wu M, Bachman H, Mesyngier N, et al. Enriching nanoparticles via acoustofluidics. ACS Nano. 2017; 11:603–12. [PubMed: 28068078]
126. Wang LV, Hu S. Photoacoustic tomography: in vivo imaging from organelles to organs. Science. 2012; 335:1458–62. [PubMed: 22442475]
127. Beard P. Biomedical photoacoustic imaging. Interface Focus. 2011; 1:602–31. [PubMed: 22866233]

128. Yao J, Wang L, Yang J-M, Maslov KI, Wong TTW, et al. High-speed label-free functional photoacoustic microscopy of mouse brain in action. Nat Methods. 2015; 12:407–10. [PubMed: 25822799]
129. Staley J, Grogan P, Samadi AK, Cui H, Cohen MS, Yang X. Growth of melanoma brain tumors monitored by photoacoustic microscopy. J Biomed Opt. 2010; 15:040510. [PubMed: 20799777]
130. Zhang HF, Maslov K, Sivaramakrishnan M, Stoica G, Wang LV. Imaging of hemoglobin oxygen saturation variations in single vessels *in vivo* using photoacoustic microscopy. Appl Phys Lett. 2007; 90:053901.
131. Jathoul AP, Laufer J, Ogunlade O, Treeby B, Cox B, et al. Deep *in vivo* photoacoustic imaging of mammalian tissues using a tyrosinase-based genetic reporter. Nat Photonics. 2015; 9:239–46.
132. Weber J, Beard PC, Bohndiek SE. Contrast agents for molecular photoacoustic imaging. Nat Methods. 2016; 13:639–50. [PubMed: 27467727]
133. Cai X, Li L, Krumholz A, Guo Z, Erpelding TN, et al. Multi-scale molecular photoacoustic tomography of gene expression. PLOS ONE. 2012; 7:e43999. [PubMed: 22952846]
134. Yao J, Kaberniuk AA, Li L, Shcherbakova DM, Zhang R, et al. Multi-scale photoacoustic tomography using reversibly switchable bacterial phytochrome as a near-infrared photochromic probe. Nat Methods. 2016; 13:67–73. [PubMed: 26550774]
135. Yaqoob Z, Psaltis D, Feld MS, Yang C. Optical phase conjugation for turbidity suppression in biological samples. Nat Photonics. 2008; 2:110–15. [PubMed: 19492016]
136. McDowell EJ, Cui M, Vellekoop IM, Senekerimyan V, Yaqoob Z, Yang C. Turbidity suppression from the ballistic to the diffusive regime in biological tissues using optical phase conjugation. J Biomed Opt. 2010; 15:025004–11. [PubMed: 20459245]
137. Vellekoop IM, van Putten EG, Lagendijk A, Mosk AP. Demixing light paths inside disordered metamaterials. Opt Express. 2008; 16:67–80. [PubMed: 18521133]
138. Mahan G, Engler W, Tiemann J, Uzgiris E. Ultrasonic tagging of light: theory. PNAS. 1998; 95:14015–19. [PubMed: 9826644]
139. Xu X, Liu H, Wang LV. Time-reversed ultrasonically encoded optical focusing into scattering media. Nat Photonics. 2011; 5:154–57. [PubMed: 21532925]
140. Wang YM, Judkewitz B, DiMarzio CA, Yang C. Deep-tissue focal fluorescence imaging with digitally time-reversed ultrasound-encoded light. Nat Commun. 2012; 3:928. [PubMed: 22735456]
141. Judkewitz B, Wang YM, Horstmeyer R, Mathy A, Yang C. Speckle-scale focusing in the diffusive regime with time reversal of variance-encoded light (TROVE). Nat Photonics. 2013; 7:300–5. [PubMed: 23814605]
142. Shapiro MG, Ramirez RM, Sperling LJ, Sun G, Sun J, et al. Genetically encoded reporters for hyperpolarized xenon magnetic resonance imaging. Nat Chem. 2014; 6:629–34. [PubMed: 24950334]
143. Lu GJ, Farhadi A, Szablowski JO, Lee-Gosselin A, Barnes SR. , et al. Acoustically modulated magnetic resonance imaging of gas-filled protein nanostructures. Nat Mater. 2018. In press.

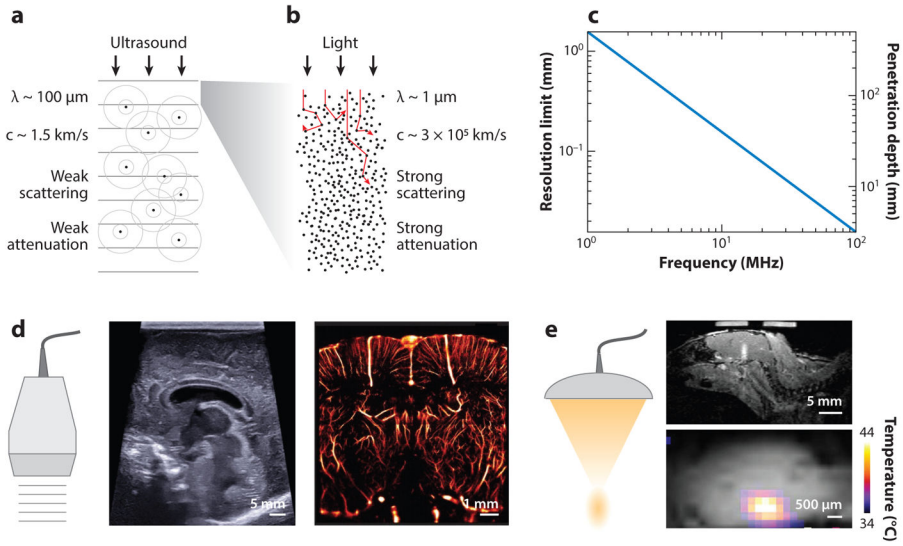

Figure 1.

Properties and applications of ultrasound waves. (*a*) Physical properties of ultrasound waves in biological tissues. (*b*) Physical properties of light traveling in biological tissue. (*c*) Fundamental tradeoff between ultrasound resolution and penetration depth as a function of frequency in brain tissue (penetration depth was assessed based on a 60-decibel round-trip attenuation). At an ultrasound frequency of 15 MHz, one can expect to image the brain 2 cm deep at a 100-μm resolution. (*d*) Illustration of ultrasound imaging capabilities; conventional B-mode image of an infant brain with a submillimeter resolution of cerebral structures; 15-MHz superresolution ultrasound image of the rat brain vasculature with an 8-μm resolution, breaking the classical tradeoff exposed in *c* [adapted with permission from Errico et al. (18)]. (*e*) Illustration of focused ultrasound energy delivery with millimeter precision. (*top*) Local blood-brain barrier opening induced by stable microbubble cavitation and tracked with gadolinium-enhanced magnetic resonance image (MRI); (*bottom*) MRI temperature map of a phantom during focused ultrasound insonification.

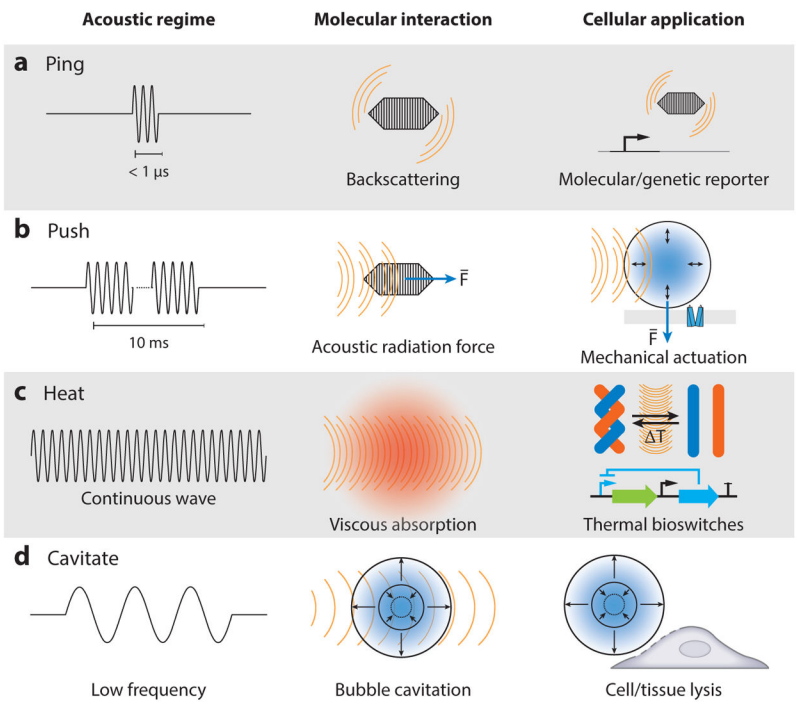

Figure 2.

Regimes of biomolecular ultrasound. (*a*) Short ultrasound pulse backscattering is used to image acoustic biomolecules in vivo. (*b*) Extended ultrasound pulses induce an acoustic radiation force that can actuate ultrasound-sensitive particles. (*c*) Continuous ultrasound waves lead to local heating and can be used to turn on thermal bioswitches. (*d)* Low-frequency ultrasound can be used to cavitate microbubbles that can induce cell or vascular barrier disruption.

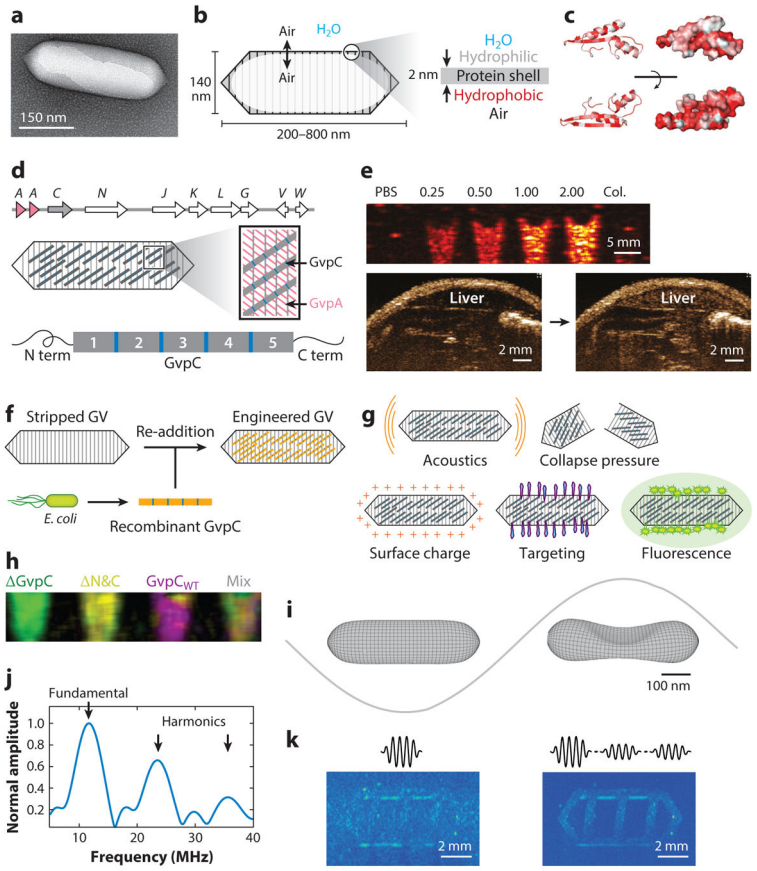

Figure 3.

Gas vesicles as acoustic biomolecules. (*a*) Transmission electron micrograph of individual gas vesicle (GV) from *Anabaena flos-aquae*. (*b*) Illustration of GV structure. (*c*) Protein folding model for *A. flos-aquae* gas vesicle protein A (GvpA), colored to indicate hydrophobicity (*red*). Structure from Ezzeldin et al. (40), rendered in PyMOL. (*d*) Gene cluster encoding *A. flos-aquae* GVs (*top*), illustration of GvpA and GvpC spatial arrangement (*middle*), and repeat structure of GvpC protein (*bottom*). (*e*) Ultrasound image of GVs at various optical densities and after hydrostatic collapse in vitro. Image of mouse during and after GV administration in vivo, showing contrast in the liver owing to GV accumulation. (*f*) Illustration of protocol for replacing native GvpC with engineered versions. (*g*) GV properties that can be modified by substituting engineered versions of GvpC. (*h*) Multiplexed image of engineered GVs acquired with pressure spectral unmixing. (*i*) Finite element model of *A. flos-aquae* GV buckling under acoustic pressure. (*j*) Predicted acoustic output from buckling GVs. (*k*) B-mode and amplitude modulated images of gas vesicles arranged in a phantom with linear background scatterers. Panel *a* adapted with permission from Lu et al. (143). Panels *d*, *f–h* adapted with permission from Lakshmanan et al. (43). Panel *e* adapted with permission from Shapiro et al. (35). Panels *i–k* adapted with permission from Maresca et al. (45).

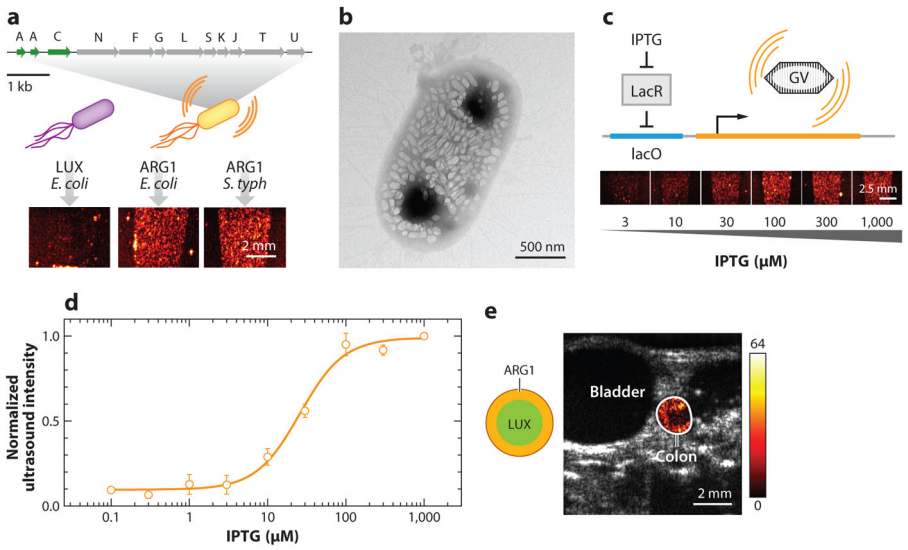

Figure 4.

Acoustic reporter genes. (*a*) Diagram of engineered ARG1 gene cluster encoding gas vesicle protein A (GvpA) and GvpC from *Anabaena flos-aquae* and GvpN–U from *Bacillus megaterium* (*top*), resulting in ultrasound contrast when expressed in *Escherichia coli* or *Salmonella typhimurium* (*bottom*), compared with bacteria expressing the LuxABCDE operon. (*b*) Transmission electron microscopy image of *E. coli* Nissle 1917 expressing ARG1. (*c*) Illustration of engineered circuit in which ARG expression is driven by a chemical inducer (*top*), and ultrasound images of *E. coli* after induction with different amounts of the inducer [isopropyl β-D-1-thiogalactopyranoside (IPTG), *bottom*]. (*d)* Normalized ultrasound signal intensity from bacteria induced with different amounts of the inducer, showing the expected circuit output. (*e*) Anatomical (*gray*) and background-subtracted contrast (*hot colormap*) ultrasound image of mouse with colon containing *E. coli* Nissle 1917 expressing either ARG1 or LuxABCDE in the indicated spatial arrangement. Panels *a–e* adapted with permission from Bourdeau et al. (46).

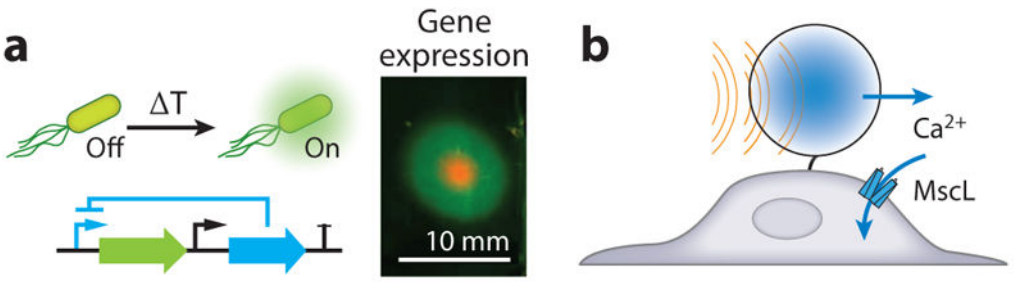

Figure 5.

Biomolecular applications of focused ultrasound. (*a*) Schematic of thermal bioswitch controlling gene expression and in vitro patterned gene expression in the region targeted by focused ultrasound. (*b*) Mechanical actuation of a mechanosensitive channel by exerting acoustic radiation force on a microbubble. Panel *a* adapted with permission from Piraner & Abedi (71).

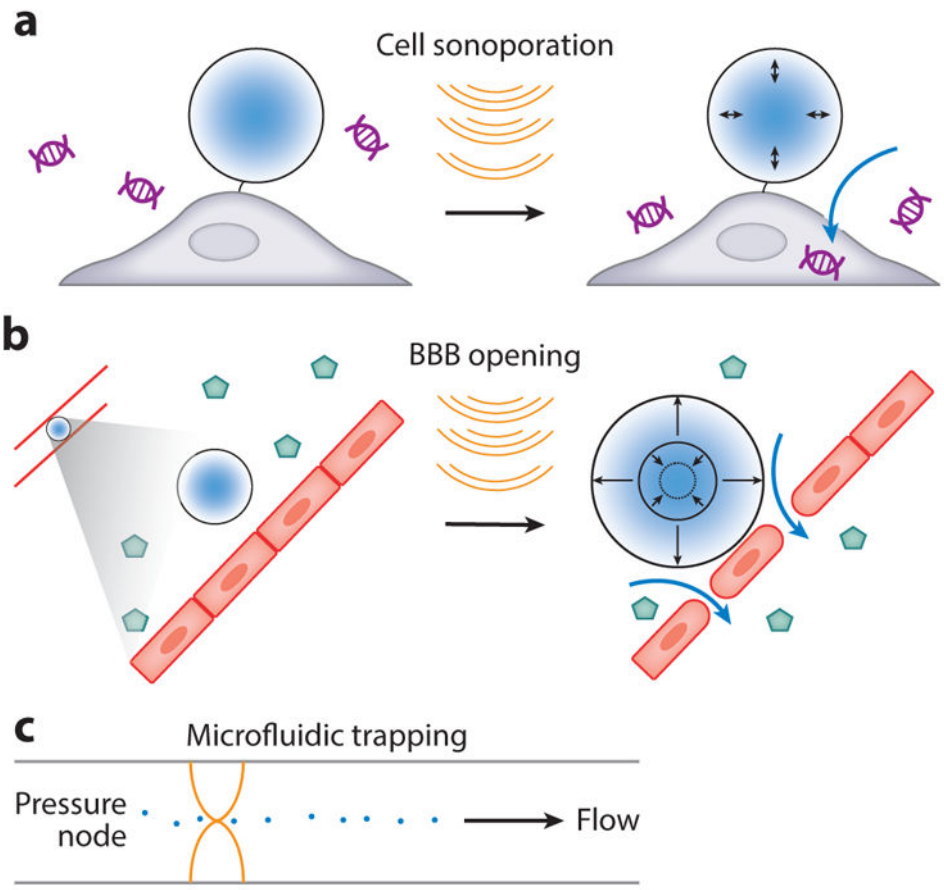

Figure 6.

Biomolecular transport using ultrasound. (*a*) Sonoporation of a cell with a bubble, enabling DNA uptake. (*b*) Microbubble vibration induces loosening of vascular tight junctions, enabling virus uptake through the blood-brain barrier (BBB). (*c*) Acoustic trapping of particles in a microfluidic channel with standing ultrasound waves.